View metadata, citation and similar papers at core.ac.uk

brought to you by CORE

provided by Explore Bristol Research

Renson, L., Ehrhardt, D. A., Barton, D. A. W., Neild, S. A., & Cooper, J. E. (2016). Connecting Nonlinear Normal Modes to the Forced Response of a Geometric Nonlinear Structure with Closely Spaced Modes. In 2016 11th International Symposium on Mechatronics and its Applications (ISMA 2016): Proceedings of a meeting held 19-21 September 2016, Leuven, Belgium. Institute of Electrical and Electronics Engineers (IEEE).

Peer reviewed version

Link to publication record in Explore Bristol Research

PDF-document

University of Bristol - Explore Bristol Research

General rights

This document is made available in accordance with publisher policies. Please cite only the published version using the reference above. Full terms of use are available:
http://www.bristol.ac.uk/pure/about/ebr-terms.html

Connecting Nonlinear Normal Modes to the Forced Response of a Geometric Nonlinear Structure with Closely Spaced Modes

L. Renson, D. A. Ehrhardt, D. A. W. Barton, S. A. Neild, and J. E. Cooper
Faculty of Engineering, University of Bristol, Bristol, UK.
e-mail: **l.renson@bristol.ac.uk**

Abstract
This paper numerically and experimentally investigates the relationship between the nonlinear normal modes and the forced response of a clamped-clamped cross beam structure. The system possesses closely-spaced linear modes such that the applied force distribution across the structure plays a central role in the appropriation of the nonlinear normal modes. Numerical simulations show that the quadrature conditions of the forced response does not necessarily match the peak response nor the nonlinear normal modes of the underlying conservative system, but instead are dependent upon the applied excitation. Experimental investigations performed with a single-point excitation and control based continuation further demonstrate the necessity for appropriate forcing in order to extract the NNMs of such systems.

1 Introduction

Vibration modes play an important role in the design of mechanical structures as they govern the structure's preferred deformation shapes and the resonance frequencies at which the system is particularly sensitive to external excitations. For nonlinear systems, resonance frequencies and modes shapes vary as a function of the vibration amplitude [1, 2]. This evolution can be captured by nonlinear normal modes (NNMs).

In analogy with linear normal modes (LNMs), the resonances of a weakly-damped nonlinear system occur in the neighborhood of its NNMs. More precisely, it was proved that a forced damped system can oscillate according to the NNMs of its underlying conservative system provided that a multi-harmonic excitation in phase quadrature with the response is applied to all the degrees of freedom of the system [3]. The appropriate selection of the input force distribution (both spatially and harmonically) permits the counterbalance of the damping in the structure and the isolation of a specific NNM. Several techniques exploit this result to directly measure NNMs during experimental tests. For instance, the NNMs of a nonlinear beam, spring-mass system, a wing-pylon structure, and steel frame structure were extracted using a method termed resonant decay in Refs. [4, 5, 6, 7], respectively. In Refs. [8, 9], the NNMs of a nonlinear tuned mass damper and of a energy harvester were extracted using the control-based continuation method which is also implemented in the present work. In the above experiments, the minimal nonlinear coupling allowed the simplification of the input force to a single-point single-harmonic excitation while still successfully capturing the system NNMs. In Ref. [10], a system with symmetric but harmonically couple modes was considered, and a single-point multi-harmonic excitation was required to isolate NNMs.

The present work investigates the resonant dynamics of a system with two closely-spaced modes (i.e. coupled in the fundamental harmonic). For such systems, the amplitude and spatial distribution of the excitation across the structure can strongly influence the ability to observe the NNMs of the system. Different forcing configurations can lead to vastly different forced response curves and resonance peaks. Furthermore, as a consequence of inappropriate forcing, the phase quadrature achieved between the excitation and the response

does not necessarily correspond to a resonance peak or a NNM of the underlying conservative system. These results can have strong practical implications if one wants to measure NNMs during experimental tests.

Experimental investigations are conducted on a clamped-clamped cross beam. The thickness of the clamped-clamped beam is relatively small compared to its length such that the system features geometric nonlinearities with predominantly hardening characteristics when under large amplitude planar deformations. The NNMs of the physical structure are studied experimentally using the method developed in Ref. [8]. Exploiting the concept of control-based continuation (CBC), this method combines stabilizing feedback control and path following techniques to track in the experiment the steady-state periodic responses describing the NNMs of the system. The distribution of the applied input force will appear particularly important for the method. The particular case of a single-point forcing that essentially excites one the LNMs of the underlying linear structure is considered in order to show the limitations introduced by inappropriate forcing. In particular, quadrature conditions will no longer be reached and the CBC method will fail to control the system dynamics as the unexcited LNM gains importance in the response.

The paper is organized as follows. The system studied in the paper is presented in Section 2, together with its linear properties which are experimentally identified. Numerical investigations are presented in Section 3. A reduced-order model of the structure is built using the implicit condensation and expansion method [11]. The NNMs of the underlying conservative system are discussed. The theory for nonlinear force appropriation is briefly reviewed in Section 3.3 and the connections that exist between the system NNMs and forced response is investigated for different forcing configurations. In Section 4 the NNMs of the physical system are experimentally measured. Conclusions are discussed in Section 5.

2 The physical system

The structure under consideration was created to exhibit close natural frequencies between the first bending and first torsion mode of vibration. The final design consists of two beams (the main beam and the cross beam) joined in the middle and a third smaller beam connected to the main beam as seen in Fig. 1. The main beam is clamped at both ends. The cross beam is welded to the main beam and two concentrated masses are attached at both ends with set screws so the masses remain adjustable (i.e. change in the cross beam symmetry and inertia is permitted). The third beam (force cross beam) was also welded to the main beam to facilitate multi-input testing and the excitation of the first torsion mode; however, this is not utilized in this work. The main beam's dimensions are l x w x h of 1000mm x 12mm x 6mm, the cross beam's dimensions are l x d of 410mm x 12mm, and the force cross beams dimensions are l x w x h 150mm x 15mm x 15mm. The dimensions of the concentrated masses are d x h of 38 mm x 24 mm.

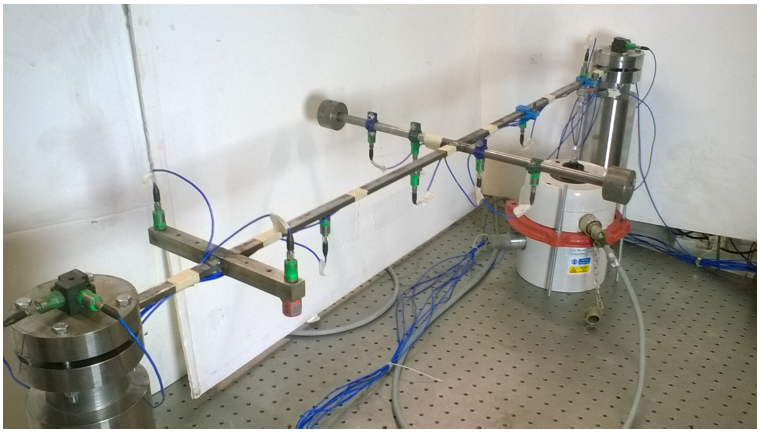

Figure 1: Clamped-clamped cross beam.

2.1 Linear modal testing

The clamped-clamped cross beam structure presented in Figure 1 was first investigated using multi-input multi-output impact hammer tests in order to extract its underlying linear properties. The shaker later used for measuring NNMs was disconnected from the structure in order to discard its influence on the stiffness and damping properties of the structure. The positions of the localized masses were adjusted such that the first two natural frequencies are approximately 0.5 Hz apart while breaking the torsion mode symmetry to avoid veering [12]. The two first natural frequencies and damping ratios of the final configuration are reported in Table 1. The associated modal shapes are sketched in Figure 2. Although both modes combine bending and torsion components, the first mode is dominated by a bending motion (Fig. 2(a)) whereas the second one is dominated by torsion (Fig. 2(b)).

	Mode 1	Mode 2
Frequency (Hz)	15.67	16.18
Damping ratio (%)	0.11	0.26

Table 1: Resonance frequencies and damping ratios identified from impact-hammer data.

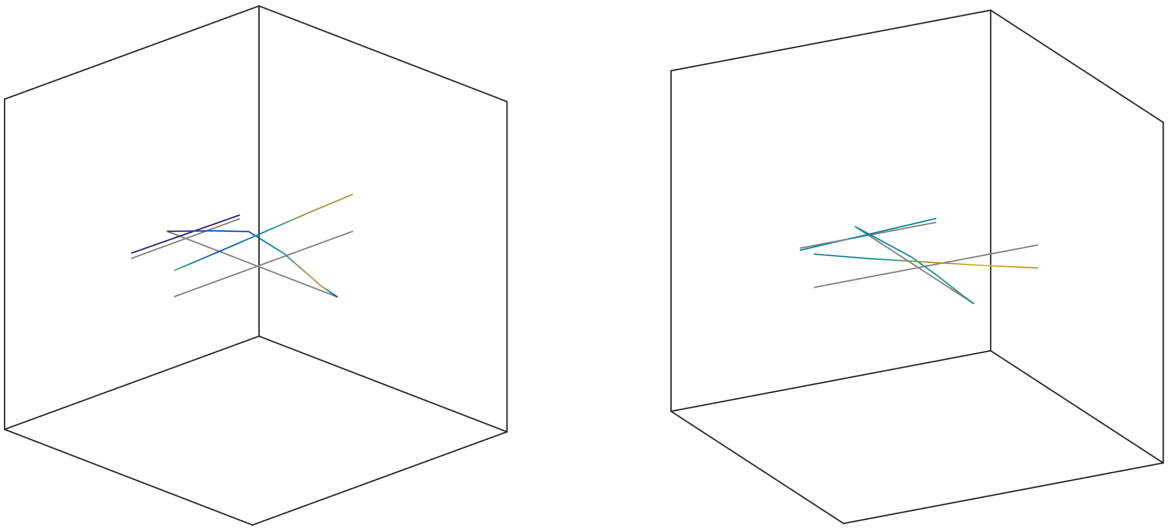

(a) (b)

Figure 2: Linear mode shapes identified from impact-hammer data.

3 Numerical simulations

3.1 Reduced-order model

A finite element model of the structure in Fig. 1 was created in Abaqus. A total of 266 B31 beam elements were used to discretise the cross sections of all beams as well as the concentrated masses at the tip of the cross beam. The boundary conditions of the main beam are also modeled using linear axial springs whose stiffness coefficients were determined from static force-displacement tests prior to clamping. The resulting model contains 1596 degrees of freedom and appears to be stiffer than the physical system. The first and second natural frequencies are overestimated by 1.55 Hz and 1.33 Hz, respectively.

Performing nonlinear dynamic analysis on this size of a model can be time consuming. Therefore a non-linear reduced order model (NLROM) was created using the implicit condensation and expansion method

(ICE) [11]. In this method, the expected nonlinear stiffening effects due to large amplitudes of deformation are implicitly accounted for using nonlinear static solutions in Abaqus. Using specific levels of applied modal forces, the resulting deformation is decomposed onto a preselected modal reduction basis, and the nonlinear stiffness coefficients are determined based on the resulting restoring force and modal displacement relationship. The ICE method produces an N DOF system of equations in the modal domain as

$$\ddot{\mathbf{q}} + \mathbf{\Lambda}\mathbf{q} + \mathbf{N}_{\mathbf{q}}(\mathbf{q}) = \mathbf{0}, \tag{1}$$

where $\mathbf{q}$ stands for the linear modal coordinates. Since this work focuses on the coupling between the two first fundamental modes, Eq. (1) can be summarized to a 2-DOF system with $\mathbf{q} = [q_1\ q_2]^{\mathrm{T}}$, $\mathbf{\Lambda} = \mathrm{diag}(\omega_1^2,\ \omega_2^2)$, and

$$\mathbf{N}_{\mathbf{q}}(\mathbf{q}) = \begin{pmatrix} \alpha_1 q_1^2 + 2\alpha_2 q_1 q_2 + \alpha_3 q_2^2 + \gamma_1 q_1^3 + 3\gamma_2 q_1^2 q_2 + \gamma_3 q_1 q_2^2 + \gamma_4 q_2^3 \\ \alpha_2 q_1^2 + 2\alpha_3 q_1 q_2 + \alpha_4 q_2^2 + \gamma_2 q_1^3 + \gamma_3 q_1^2 q_2 + 3\gamma_4 q_1 q_2^2 + \gamma_5 q_2^3 \end{pmatrix}. \tag{2}$$

In linear response regimes the system response can be well approximated as uncoupled using the linear modes of vibration; however, in nonlinear response regimes, the system response now includes both modes of interest (coupled through $\mathbf{N}_{\mathbf{q}}(\mathbf{q})$). The 2-DOF NLROM created using the ICE method is used to find the NNMs and study the forced response of the structure as described in Sections 3.2 and 3.4.

3.2 Nonlinear normal modes

In this work, NNMs are defined as non-necessarily synchronous periodic solutions of the conservative equations of motion (1). A number of numerical algorithms were developed to compute NNMs, as recently reviewed in Ref. [13]. The method considered here combines shooting and pseudo-arclength continuation techniques and is freely available in the so-called NNMcont software package [14].

The NNMs of this structure exhibit strong coupled dynamic motions between the bending- and torsion-dominated LNMs as seen in Fig. 3. At low energies, the deformation of the first NNM (NNM1) and second NNM (NNM2) match the corresponding LNM shapes. At higher response energies, the NNM deformations exhibit a veering phenomenon where the deformations are an equal combination of the underlying LNMs, but are separated by 0.13 Hz. As the response is pushed passed the region of veering, the deformation of NNM1 resembles the torsion dominated LNM (i.e. LNM2) and NNM2 resembles the bending dominated LNM shape (i.e. LNM1).

The change in the deformation of the NNMs can also be examined in terms of the first and second LNM amplitude (Figs. 4(a, b)). For frequencies close to the linear natural frequencies, the amplitude of LNM1 dominates the response of NNM1 whereas the amplitude of LNM2 dominates NNM2. As frequency increases, the LNM contributions to the NNMs are swapped such that NNM1 is dominated by LNM2 and NNM2 by LNM1.

3.3 Nonlinear force appropriation

The forced damped dynamics of system (1) can be written in linear modal space as

$$\ddot{\mathbf{q}} + \mathbf{\Xi}\dot{\mathbf{q}} + \mathbf{\Lambda}\mathbf{q} + \mathbf{N}_{\mathbf{q}}(\mathbf{q}) = \mathbf{p}, \tag{3}$$

where $\mathbf{\Xi} = \mathrm{diag}(2\zeta_1\omega_1,\ 2\zeta_2\omega_2)$ is the modal damping matrix and $\mathbf{p}$ is the modal forcing vector. As was done in Refs. [15, 10, 16], the energy balance technique can be used to find the multi-point multi-harmonic input force $\mathbf{p}$ that puts the same amount of energy into the structures ($E_{\text{in/cycle}}$) as is dissipated by damping ($E_{\text{diss./cycle}}$). Considering the structure response $\mathbf{q}_{\text{nnm}}(t)$ at a given NNM, the balance between the input and dissipated energy per cycle writes

$$\int_0^T \dot{\mathbf{q}}_{\text{nnm}}^{\mathrm{T}} \mathbf{\Xi} \dot{\mathbf{q}}_{\text{nnm}} dt = \int_0^T \dot{\mathbf{q}}_{\text{nnm}}^{\mathrm{T}} \mathbf{p} = \sum_k \int_0^T \dot{\mathbf{q}}_{\text{nnm}}^{\mathrm{T}} \mathbf{c}_k \sin(k\omega t), \tag{4}$$

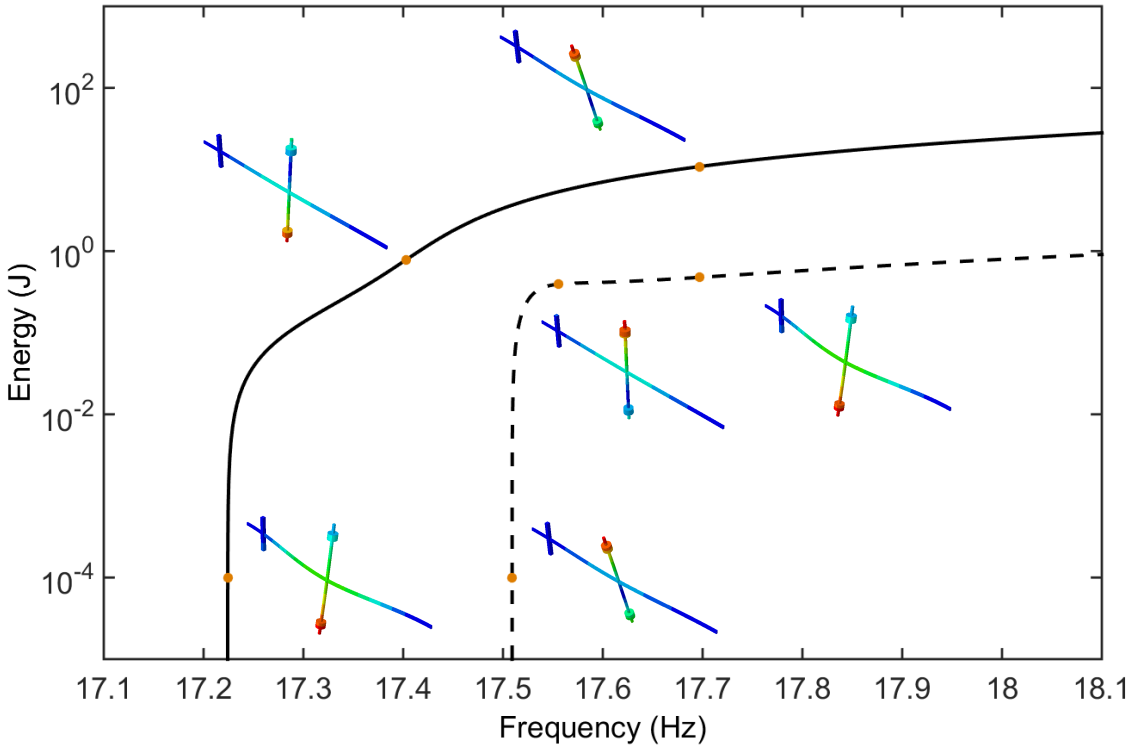

Figure 3: Frequency-energy plot of the nonlinear normal modes of the clamped-clamped cross beam structure ROM. (–) First NNM; (– –) second NNM. Mode shapes are inset.

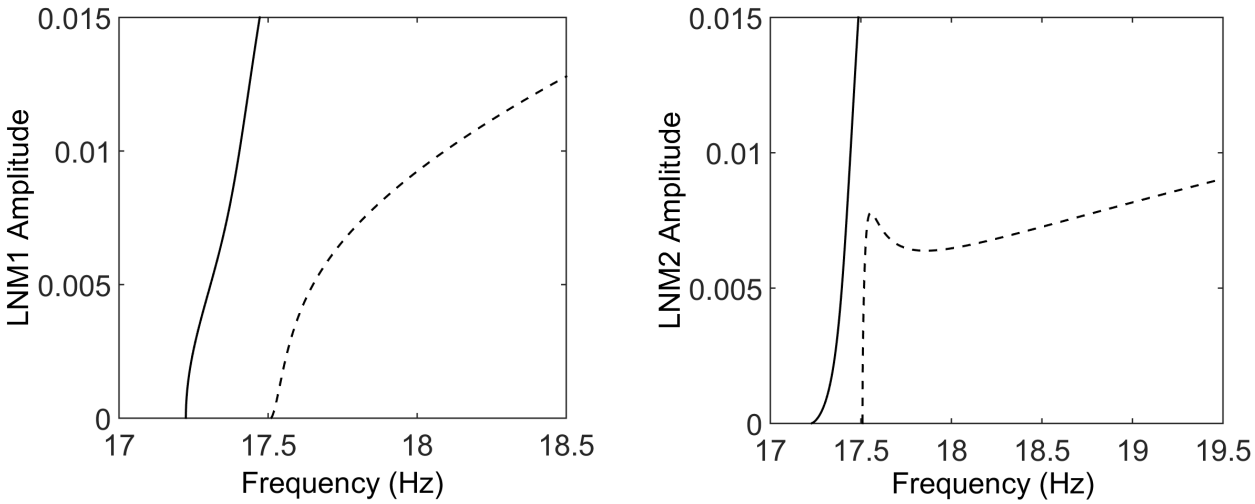

Figure 4: Amplitude of the first (a) and second (b) linear modal coordinates for the nonlinear normal modes of the clamped-clamped cross beam structure. (–) First NNM; (– –) second NNM.

where the second equality is obtained by fixing the phase of the periodic excitation and $\mathbf{c}_k$ is the force amplitude vector at the harmonic k. Equation (4) is exploited in Section 3.4 to estimate the forcing coefficients $\mathbf{c}_k$ required to balance the damping introduced by $\boldsymbol{\Xi}$ when the system oscillates according to one of its NNM. In practice, the NNM is not known a priori, so one generally has to tune the input force until the phase quadrature condition is met.

3.4 Comparison between the NNMs and the forced response

The particular case of an ideal force distribution as given by Equation (4) is studied before investigating other input force distributions.

The appropriate force is calculated for NNM1 at several response amplitudes. The modal force vector $\mathbf{p}^{\mathrm{T}} = [p_1 \ p_2]$ includes contributions from both LNMs ($p_1 \neq 0$ and $p_2 \neq 0$) due to the coupling introduced by nonlinearity. The response in LNM1 and LNM2 is reported in Figure 5(a) and 5(b), respectively. The agreement between the peak response, the quadrature condition and the backbone curve of NNM1 (solid-black) is excellent. The presence of a LNM2 component in the forcing leads to the presence of a second resonance peak and a phase quadrature condition around NNM2 (Figure 5(b)). Such a peak and phase transition are not visible in the response of LNM1 because the response regimes for which NNM2 includes significant LNM1 contributions are not yet reached.

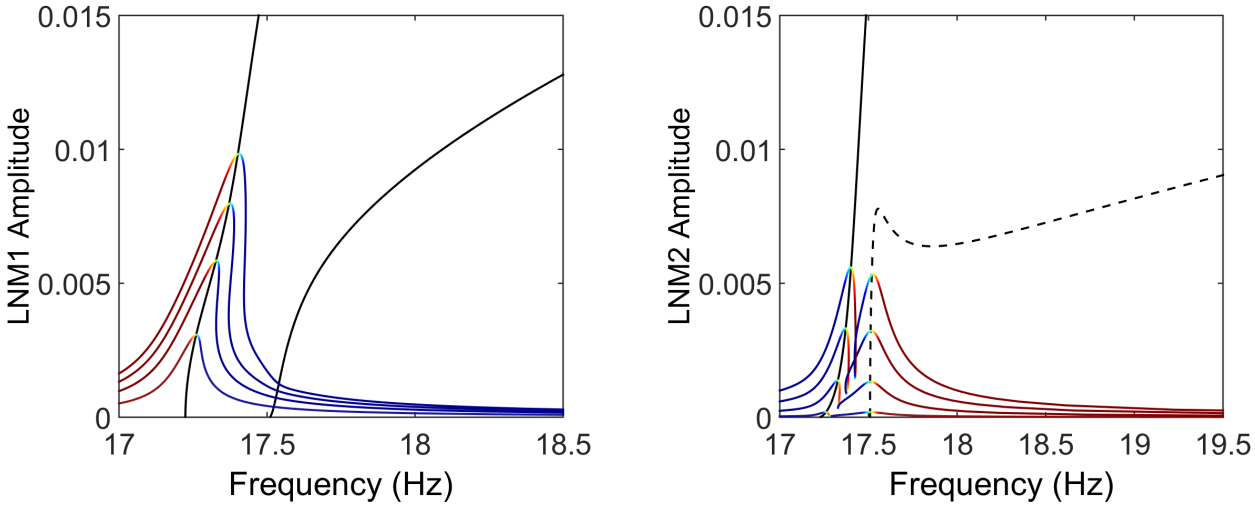

Figure 5: Amplitude of the first (a) and second (b) linear modal coordinates for the nonlinear normal modes of the clamped-clamped cross beam structure. First (–) and second (– –) NNM backbone curve. The colour code represents the phase lag ϕ between the LNM response and the excitation. Blue: $\phi < 89.7°$; green: $\phi = 90°$; red: $\phi > 90.3°$.

The particular case of an excitation applied to a single LNM is now investigated. Figure 6(a, b) shows for three force amplitudes the response of the structure when the excitation is distributed according to LNM1 (i.e., $\mathbf{p}^{\mathrm{T}} = [p_1 \ 0], \ p_1 \neq 0$). The response in LNM1 (Fig. 6(a)) shows a first resonance peak close to NNM1 backbone curve. For the low-amplitude response curve, the NNM, the phase quadrature condition, and the resonance peak are all in good agreement with each other. For larger response amplitudes, however, the NNM starts to deviate from the peak response and the quadrature condition no longer lines up with the peak amplitude nor the NNM. This is a direct consequence of the absence of LNM2 components in the excitation. Similar observations are made when looking at the response in LNM2 (Figure 6(b)). Although NNM1 and the phase quadrature condition are in good agreement, they do not match the forced response resonance peak.

As seen in Section 3.2, the second NNM can contain strong LNM1 contributions when at high vibration amplitudes (see Figure 3). This leads to the presence of a resonance peak around NNM2 backbone curve for high-amplitude responses (Figure 6(a)).

The high-amplitude response curve in Figure 6(a) shows a second phase transition, occurring between the first and second resonance peak. This transition is the consequence of a Neimark-Sacker bifurcation at which periodic solutions lose stability and quasi-periodic oscillations become visible. This phenomenon

was already numerically and experimentally observed for this structure in Ref. [17]. The resonant response around NNM2 is not visible for the first two force levels. It is in fact detached from the main forced response curve and would therefore form loops of isolated solutions in Figures 6(a) and 6(b) (not represented here for clarity).

The response of the structure in LNM2 (Figure 6(b)) clearly highlights the presence of the coupling terms between LNM1 and LNM2 introduced by nonlinearity. If the structure was linear, LNM2 response would be identically zero and the second resonance peak in (Figure 6(a)) would be absent. A consequence of this coupling is that a quadrature condition at NNM2 can be reached at low amplitude, i.e. when NNM2 is dominated by LNM2. However, this quadrature region does not correspond to any resonance peak.

The response of the structure to a forcing in LNM2 ($\mathbf{p}^{\mathrm{T}} = [0 \ p_2], \ p_2 \neq 0$) is presented in Figure 6(c, d). The intermediate-amplitude response curve in LNM2 presents a first resonance peak located between NNM1 and NNM2 backbone curves. Furthermore, this peak does not correspond to any phase transition in the forced response. For higher response amplitudes, the increasing importance of LNM2 in NNM1 (cf. Section 3.2) leads to a resonance peak and a quadrature condition that matches well the backbone curve of NNM1. At this force level, LNM1 also shows a resonance peak close to NNM1. The disagreement between the resonance peak and NNM comes from the absence of LNM1 contributions in the applied force. Furthermore, the solution curve does not present any clear phase transition. This shows that excited modes (equivalently, degrees of freedom) can be in quadrature with the excitation whereas the other modes (DOFs) are not.

4 Experimental results

To demonstrate the importance of the applied excitation in the experimental identification of NNMs, the structure was tested using a single shaker attached to the main beam, providing pure bending excitation. The CBC technique described in Ref. [8] was used to measure the NNMs of the structure. The method combines feedback control and path following techniques in order to follow the steady-state responses of the system as parameters are varied. In this paper, the CBC method was exploited to track the periodic responses that are in quadrature with the excitation as a function of the response amplitude. The $\frac{\pi}{2}$-quadrature condition was experimentally reached within ± 0.005 rad.

The feedback control system considered in CBC was a simple linear proportional-plus-derivative feedback control system with fixed gains. The reference signal was chosen as the velocity integrated from an accelerometer located on the cross beam in order to capture both bending and torsion motions. The obtained velocity signal was high-pass filtered using a fourth-order Butterworth filter in order to remove the DC component introduced by time integration. The filter cut-off frequency was chosen at 8 Hz, which represented a good compromise between the introduced delay and the stability of the filter. Proportional and derivative gains were kept constant and equal to 0.5 and -0.0025 throughout the tests.

Fig. 7(a) shows in a response frequency – response amplitude plot the first NNM (–) and second NNM (– –) of the clamped-clamped cross beam. For both NNMs, the resonance frequency of the smallest-amplitude data point is in good agreement with the linear natural frequencies identified using impact-hammer data (see Table 1). This shows that CBC has discarded effectively the influence of the excitation system. Up to approximately 20 m/s^2, the resonance frequency of both NNMs decreases for increasing vibration amplitudes. This is attributed to gravity-induced static deformations and imperfect clamping boundary conditions. For vibration amplitudes larger than 20 m/s^2, the geometrical coupling that exists between the bending and axial beam deformations introduces hardening nonlinearities and the resonance frequencies increase, as theoretically predicted and modeled in Section 3.2.

Both NNMs presented in Fig. 7(a) are incomplete and could only be captured in regions where the response is dominated by bending motions. This is clearly illustrated in Figure 7(b) where both NNMs are projected onto LNM1 and LNM2. NNM1 was captured up to approximately 16.4 Hz, frequency at which the LNM1 (i.e.

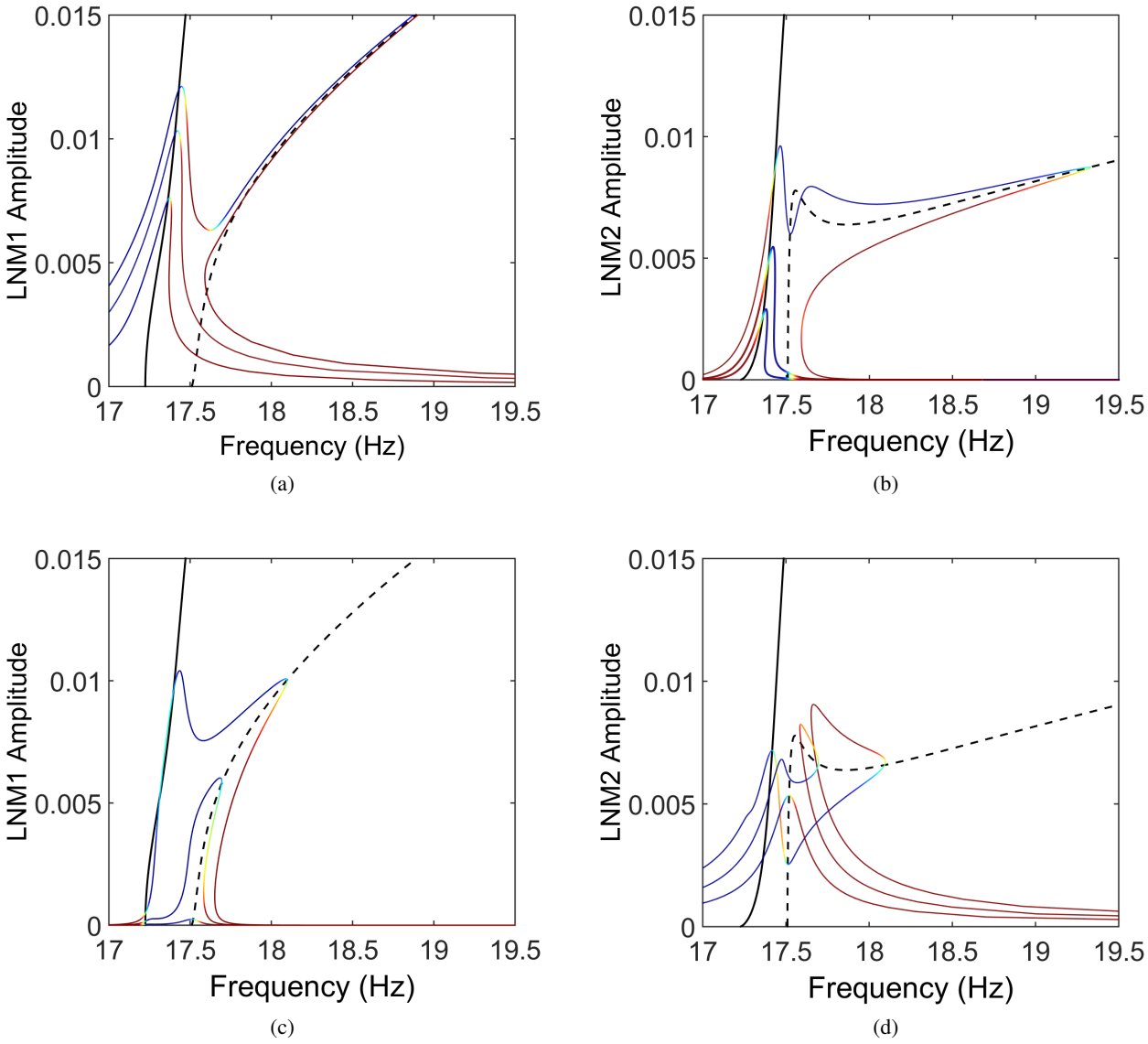

Figure 6: Forced response curves for an input force distributed according to LNM1 (a, b) and LNM2 (c, d). First (–) and second (– –) NNM backbone curve. The colour code represents the phase lag ϕ between the LNM response and the excitation. Blue: $\phi < 89.7°$; green: $\phi = 90°$; red: $\phi > 90.3°$.

bending) contribution starts to increase less rapidly. As discussed in Section 3.2, this region is characterised by a rapid increase of LNM2 contribution, which will eventually dominate the NNM motion (see Figures 3 and 4). The quadrature condition could no longer be found beyond 16.4 Hz.

The second NNM was captured in two regions, one at low amplitudes and one at high amplitudes of vibration. As in Figure 6(b), the quadrature condition between the force and the response was achieved. However, as numerically predicted, the response appears to be primarily in LNM1 whereas it should be in LNM2. This is a consequence of the inappropriate forcing, which also prevented to find the correct identification of the quadrature conditions and trace out NNM2 for higher response amplitudes.

The theoretical investigations conducted in Section 3.2 predicts a region where NNM2's response is primarily in bending (see Figure 3). This region was reached using CBC embedded feedback control system and the NNM was then traced for decreasing vibration amplitudes. At approximately 16.6 Hz, the feedback control system used in CBC became unstable and the experiment was interrupted. This instability is the result of an

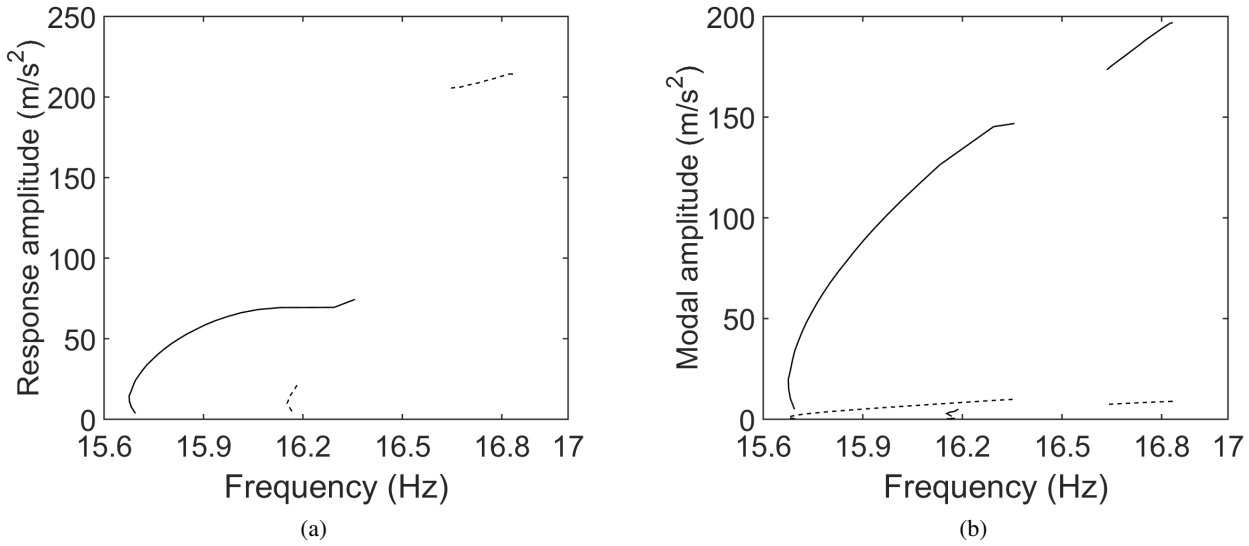

Figure 7: Backbone curves extracted experimentally using CBC. (a) Response amplitude of the accelerometer used in the feedback controller. First (–) and second (– –) NNMs. (b) Response projected on to the first (–) and second (– –) linear normal modes.

actuation applied in bending only which therefore cannot influence the torsion dynamics.

5 Conclusions

This paper provides a look at the importance of identifying the phase resonance conditions in the forced response of a nonlinear system with 1-1 coupling. Without appropriate forcing, resonance peaks will include amplitude specific coupled dynamic behavior, whereas appropriated forcing conditions provide resonance peaks which follow a NNM. This highlights an important feature needed in multi-input nonlinear force appropriation techniques.

Acknowledgements

L.R., D.A.E. are funded by the Engineering Nonlinearity EPSRC Program Grant EP/K003836/1, D.A.W.B. is funded by the EPSRC grant EP/K032738/1, S.A.N. by the EPSRC fellowship EP/K005375/1, and J.E.C. is supported by the Royal Academy of Engineering in the UK through the RAEng Airbus Sir George White Chair in Aerospace Engineering. This financial support is gratefully acknowledged.

References

[1] G. Kerschen, M. Peeters, J. C. Golinval, and A. F. Vakakis. Nonlinear normal modes, part I: A useful framework for the structural dynamicist. *Mechanical Systems and Signal Processing*, 23(1):170–194, 2009.

[2] M. Peeters, R. Viguié, G. Sérandour, G. Kerschen, and J. C. Golinval. Nonlinear normal modes, part II: Toward a practical computation using numerical continuation techniques. *Mechanical Systems and Signal Processing*, 23(1):195–216, 2009.

[3] M. Peeters, G. Kerschen, and J. C. Golinval. Dynamic testing of nonlinear vibrating structures using nonlinear normal modes. *Journal of Sound and Vibration*, 330(3):486–509, 2011.

[4] M. Peeters, G. Kerschen, and J. C. Golinval. Modal testing of nonlinear vibrating structures based on nonlinear normal modes: Experimental demonstration. *Mechanical Systems and Signal Processing*, 25(4):1227–1247, 2011.

[5] J. M. Londono, S. A. Neild, and J. E. Cooper. Identification of backbone curves of nonlinear systems from resonance decay responses. *Journal of Sound and Vibration*, 348(0):224–238, 2015.

[6] J. M. Londono, J. E. Cooper, and S. A. Neild. Identification of systems containing nonlinear stiffnesses using backbone curves. *Mechanical Systems and Signal Processing*.

[7] J. L. Zapico-Valle, M. Garcia-Diguez, and R. Alonso-Camblor. Nonlinear modal identification of a steel frame. *Engineering Structures*, 56(0):246–259, 2013.

[8] L. Renson, A. Gonzalez-Buelga, D. A. W. Barton, and S. A. Neild. Robust identification of backbone curves using control-based continuation. *Journal of Sound and Vibration*, 367:145–158, 2016.

[9] L. Renson, D.A.W. Barton, and S.A. Neild. Experimental analysis of a softening-hardening nonlinear oscillator using control-based continuation. In *Proceedings of the International Modal Analysis Conference (IMAC)*, Orlando, USA, 2016.

[10] D. A. Ehrhardt and M. S. Allen. Measurement of nonlinear normal modes using multi-harmonic stepped force appropriation and free decay. *Mechanical Systems and Signal Processing*, 7677:612–633, 2016.

[11] R. J. Kuether, B. J. Deaner, J. J. Hollkamp, and M. S. Allen. Evaluation of geometrically nonlinear reduced-order models with nonlinear normal modes. *AIAA Journal*, 53(11):3273–3285, 2015.

[12] D. A. Ehrhardt, S. A. Neild, , and J. E. Cooper. Experimental and numerical investigation of the nonlinear bending-torsion coupling of a clamped-clamped beam with centre masses. In *Proceedings of the International Modal Analysis Conference (IMAC)*, Orlando, USA, 2016.

[13] L. Renson, G. Kerschen, and B. Cochelin. Numerical computation of nonlinear normal modes in mechanical engineering. *Journal of Sound and Vibration*, 364:177–206, 2016.

[14] NNMcont - A matlab package for the computation of nonlinear normal modes. http://www.ltas-vis.ulg.ac.be/cmsms/index.php?page=nnm#package, 2014.

[15] R. J. Kuether, L. Renson, T. Detroux, C. Grappasonni, G. Kerschen, and M. S. Allen. Nonlinear normal modes, modal interactions and isolated resonance curves. *Journal of Sound and Vibration*, 351:299–310, 2015.

[16] T. L. Hill, A. Cammarano, S. A. Neild, and D. J. Wagg. Interpreting the forced response of a two-degree-of-freedom nonlinear oscillator using backbone curves. *Journal of Sound and Vibration*, 349:276–288, 2015.

[17] D. A. Ehrhardt, T. L. Hill, S. A. Neild, and J. E. Cooper. Nonlinear bending-torsion coupling of a clamped-clamped beam with tuneable masses. *Submitted*, 2016.